

Reconstructing black hole exteriors and interiors using entanglement and complexity

Wen-Bin Xu¹ and Shao-Feng Wu^{1,2}

¹*Department of Physics, Shanghai University, Shanghai 200444, China*

²*Center for Gravitation and Cosmology, Yangzhou University, Yangzhou 225009, China*

E-mail: xwb@shu.edu.cn, sfwu@shu.edu.cn

ABSTRACT: Based on the AdS/CFT correspondence, we study how to reconstruct bulk spacetime metrics by various quantum information measures on the boundary field theories, which include entanglement entropy, mutual information, entanglement of purification, and computational complexity according to the proposals of complexity=volume 2.0 and complexity=generalized volume. We present several reconstruction methods, all of which are free of UV divergence and most of which are driven by the derivatives of the measures with respect to the boundary scales. We illustrate that the exterior and interior of a black hole can be reconstructed using the measures of spatial entanglement and time-evolved complexity, respectively. We find that these measures always probe the spacetime in a local way: reconstructing the bulk metric in different radial positions requires the information at different boundary scales. We also show that the reconstruction method using complexity=volume 2.0 is the simplest and has a certain strong locality.

KEYWORDS: Bulk Reconstruction, AdS-CFT Correspondence

Contents

1	Introduction	1
2	Exterior of black holes	3
2.1	Entanglement Entropy	3
2.1.1	Holographic calculation	3
2.1.2	Reconstruction method	5
2.1.3	Example	5
2.2	Mutual Information	6
2.2.1	Holographic calculation	6
2.2.2	Reconstruction method	6
2.2.3	Example	7
2.3	Entanglement of Purification	8
2.3.1	Holographic calculation	9
2.3.2	Reconstruction method	10
2.3.3	Example	11
3	Interior of black holes	11
3.1	Complexity = Volume 2.0	12
3.1.1	Holographic calculation	12
3.1.2	Reconstruction method	13
3.1.3	Example	14
3.2	Complexity = Generalized Volume	14
3.2.1	Holographic calculation	14
3.2.2	Reconstruction method	15
3.2.3	Example	17
4	Comparison	17
5	Summary	21

1 Introduction

Anti-de Sitter/conformal field theory (AdS/CFT) correspondence not only provides a gravitational lens for strongly coupled quantum field theories but also brings a wealth of insights for quantum gravity [1–5]. The essential challenge in exploring this correspondence is to understand how the boundary degrees of freedom of the CFT can be reorganized under certain limits into the local gravitational physics in the bulk. This ambitious program is widely termed as ‘bulk reconstruction’.

Bulk reconstruction is a non-trivial inverse problem that involves holographic mapping from low to high dimensions. One of the most fascinating branches in this program is the reconstruction of the metric of the holographic spacetime¹. There are various methods regarding the bulk metric reconstruction, which use different boundary physical quantities, such as the source and expectation value of energy-momentum tensor [10], the singularities in the set of correlation functions [11, 12], the entanglement entropy (EE) of boundary intervals [13–16], the differential entropy that is a UV-finite combination of EE [17–19], the divergence structure of boundary n -point function [20, 21], the modular Hamiltonians of boundary subregions [22, 23], the Wilson loops related to quark potential [24], and four-point correlators in an excited quantum state [25], among others. It is worth noting that much of the work on metric reconstruction has been driven by the idea that spacetime is built by quantum entanglement [26–31]. However, it has been pointed out that ‘entanglement is not enough’ to encode the full spacetime [32]. In order to understand the interior of a black hole, it has been proposed that the quantum computational complexity would be important. In fact, based on the ‘complexity=volume’ (CV) proposal [32, 33], Hashimoto and Watanabe have successfully reconstructed the metric inside black holes [34].

One common challenge in computing physical quantities in quantum field theories is how to address the issue of UV divergence. In the AdS/CFT correspondence, there are systematic methods to cancel the divergence based on the UV/IR connection [4], which are well known as holographic renormalization [35, 36]. However, most of work on holographic renormalization is constrained to the standard AdS/CFT, which requires the conformal symmetry, infinite coupling, and large N limit. How to remove the divergence on gravity and field theory consistently beyond these constraints remains an open question. In light of this, ref. [37] uses the derivative of EE with respect to the spatial size of entangling region l as data, which are insensitive to the UV cutoff, unlike to EE itself. As a result, the reconstruction of metric is free of UV divergence. Note that canceling off the UV divergence has also been a guide to the correct formula for the differential entropy [17].

On the other hand, deep learning (DL) algorithms have been utilized to reconstruct the metric [38–48]. This not only unlocks the potential for building a data-driven holographic model but also provides insights into holography using the language of machine learning². In ref. [43], an interesting difference was observed between the analytical reconstruction method using the l -dependent EE as data [15] and the DL method using the frequency-dependent shear viscosity: the former ‘locally’ probes the bulk spacetime, while the latter is ‘non-local’. Here the non-local aspect is manifested through the excellent generalization capability of the deep neural network, which enable a narrow frequency to generate a wide frequency shear viscosity, using the learned complete metric as a hidden structure. Conversely, the local aspect indicates that the deeper spacetime is probed through the EE with a larger entangling region.

In this paper, we will explore the reconstruction of bulk metric using various quantum information measures on the boundary field theories. In addition to revisiting EE, we will

¹One can see other important branches in [6–9], especially the bulk operator reconstruction.

²This program has been referred as the ‘AdS/DL’ correspondence. Other related work that extracts the spacetime metric by machine learning but does not rely on AdS/CFT can be found in [49–52].

study mutual information (MI) [53] and entanglement of purification (EoP) [54], both of which are closely related to EE, as well as two candidate measures of complexity that differ from the CV proposal [55, 56]. For most of them, we will use their derivatives with respect to boundary scales as data. Moreover, we will compare how these measures encode the bulk metric. In particular, we will examine whether they always probe the spacetime in a local way.

2 Exterior of black holes

2.1 Entanglement Entropy

As a warm-up, we review the analytical reconstruction method using EE which was proposed by Bilson [15]. The relevant holographic dictionary is the Ryu-Takayanagi formula [27], by which the EE of the entangling region A on the boundary can be calculated in the bulk spacetime:

$$S = \frac{\text{Area}(\gamma_A)}{4G_N}. \quad (2.1)$$

Here G_N is Newton's constant and γ_A is the minimal surface which extends into the bulk and shares the boundary with ∂A . Afterwards, we will set $G_N = 1$ for convenience.

2.1.1 Holographic calculation

We will study a $d + 1$ -dimensional asymptotically AdS spacetime. As a proof of principle, we focus on a highly symmetric metric ansatz

$$ds^2 = \frac{1}{z^2} \left(-f(z)dt^2 + \frac{1}{f(z)}dz^2 + d\vec{x}^2 \right). \quad (2.2)$$

We set the planar horizon and boundary located at $z = 1$ and $z = 0$, respectively. On the boundary, we are interested in a spatial strip entangling region with a width l in one direction and an infinite length L in every other direction. The entangling region and minimal surface are depicted in figure 1. The area of the minimal surface is a function of l , which can be written as

$$A(l) = 2L^{d-2} \int_0^{\frac{l}{2}} \frac{1}{z^{d-1}} \sqrt{1 + \frac{z'^2}{f(z)}} dx, \quad (2.3)$$

where $z' = dz/dx$. The profile of the minimal surface can be obtained as follows. Treating $A(l)$ as an action and $z(x)$ as a generalized coordinate, one can read the Lagrangian

$$\mathcal{L}(z, z') = \frac{1}{z^{d-1}} \sqrt{1 + \frac{z'^2}{f(z)}}. \quad (2.4)$$

It leads to the Hamiltonian

$$\mathcal{H}(z, z') = z' \frac{d\mathcal{L}}{dz'} - \mathcal{L} = -\frac{z^{1-d}}{\sqrt{1 + \frac{z'^2}{f(z)}}}. \quad (2.5)$$

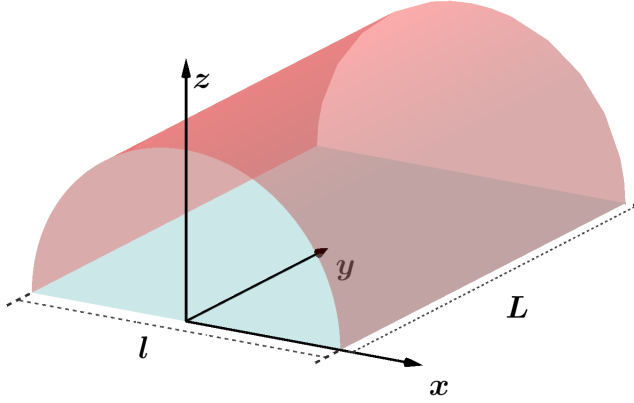


Figure 1. A minimal surface (red) in the bulk and a strip entangling region (blue) on the boundary. EE is given by the area of the red surface.

Since \mathcal{L} does not depend on the variable x explicitly, one can set \mathcal{H} as a constant

$$\mathcal{H} = -z_*^{1-d}, \quad (2.6)$$

where z_* is given by $z'|_{z=z_*} = 0$. This yields

$$\frac{dz}{dx} = \pm \frac{\sqrt{f(z)(z_*^{2d-2} - z^{2d-2})}}{z^{d-1}}. \quad (2.7)$$

Equation (2.7) with the boundary conditions $z(\pm l/2) = 0$ determines the profile function $z(x)$ for the minimal surface.

From (2.1), (2.3) and (2.7), we have

$$S(z_*) = \frac{L^{d-2}}{2} \int_{\delta}^{z_*} \frac{z_*^{d-1}}{z^{d-1} \sqrt{f(z)} \sqrt{z_*^{2d-2} - z^{2d-2}}} dz, \quad (2.8)$$

$$l(z_*) = 2 \int_0^{z_*} \frac{z^{d-1}}{\sqrt{f(z)} \sqrt{z_*^{2d-2} - z^{2d-2}}} dz, \quad (2.9)$$

where δ is the UV cutoff. Note that when $\delta \rightarrow 0$, EE is divergent. In order to cancel z_* in two equations above, we take derivatives:

$$\frac{dS(z_*)}{dz_*} = \frac{L^{d-2}}{2} \left[\frac{1}{\sqrt{f(z_*)}} \lim_{z \rightarrow z_*} \frac{1}{\sqrt{z_*^{2d-2} - z^{2d-2}}} - \int_0^{z_*} \frac{(d-1)z^{d-1}z_*^{d-2}dz}{(z_*^{2d-2} - z^{2d-2})^{\frac{3}{2}} \sqrt{f(z)}} \right], \quad (2.10)$$

$$\frac{dl(z_*)}{dz_*} = 2z_*^{d-1} \left[\frac{1}{\sqrt{f(z_*)}} \lim_{z \rightarrow z_*} \frac{1}{\sqrt{z_*^{2d-2} - z^{2d-2}}} - \int_0^{z_*} \frac{(d-1)z^{d-1}z_*^{d-2}dz}{(z_*^{2d-2} - z^{2d-2})^{\frac{3}{2}} \sqrt{f(z)}} \right]. \quad (2.11)$$

Using the chain rule

$$\frac{dS(l)}{dl} = \frac{dz_*}{dl} \frac{dS(z_*)}{dz_*}, \quad (2.12)$$

one can find

$$\frac{dS(l)}{dl} = \frac{L^{d-2}}{4z_*^{d-1}}. \quad (2.13)$$

This equation builds a relation between l and z_* .

2.1.2 Reconstruction method

The key step of Bilson's method is to solve an integral equation analytically. Referring to the handbook of integral equations [57], one can read:

$$f(x) = \int_a^x \frac{y(t)dt}{\sqrt{g(x)-g(t)}}, \quad g'(x) > 0$$

$$\text{Solution: } y(x) = \frac{1}{\pi} \frac{d}{dx} \int_a^x dt \frac{f(t)g'(t)}{\sqrt{g(x)-g(t)}}. \quad (2.14)$$

Applying eq. (2.14) to eq. (2.8), one can find

$$\frac{1}{\sqrt{f(z)}} = \frac{4(d-1)}{\pi L^{d-2}} \frac{d}{dz} \int_\delta^z \frac{S(z_*)z_*^{d-2}}{\sqrt{z^{2d-2}-z_*^{2d-2}}} dz_*. \quad (2.15)$$

This is the reconstruction formula provided by Bilson [15]. Here $S(z_*)$ is generated by the data $S(l)$ and l is related to z_* through eq. (2.13).

The analytic formula (2.15) is simple. However, the field theory data it inputs is $S(l)$, which is sensitive to the UV cutoff. Following ref. [37], we will use the derivative $S'(l)$ as the data, which is insensitive to the UV cutoff. We apply eq. (2.14) to eq. (2.9) instead of eq. (2.8), which yields a slightly different reconstruction formula³

$$\frac{1}{\sqrt{f(z)}} = \frac{d-1}{\pi z^{d-1}} \frac{d}{dz} \int_0^z \frac{l(z_*)z_*^{2d-3}}{\sqrt{z^{2d-2}-z_*^{2d-2}}} dz_*. \quad (2.16)$$

2.1.3 Example

We can check the validity of the reconstruction formula (2.16) with a simple example. We choose the AdS black hole with $d = 2$ and the function $f(z) = 1 - z^2$ as our target metric. Referring to the result of [58], the EE of a strip of width l is given by

$$S(l) = \frac{1}{2} \log \left[\frac{2}{\delta} \sinh \left(\frac{l}{2} \right) \right]. \quad (2.17)$$

In our task of bulk reconstruction, the metric is unknown but we are supposed to know

$$S'(l) = \frac{1}{4} \coth \left(\frac{l}{2} \right). \quad (2.18)$$

Combining the data with (2.13), we find

$$l(z_*) = 2 \operatorname{arctanh}(z_*). \quad (2.19)$$

This formula indicates that when l increases, the top of the geodesic probes the deeper spacetime near the horizon. We visualize the probing way in figure 2. At last, substituting (2.19) into (2.16) with $d = 2$, we recover our target metric analytically

$$f(z) = 1 - z^2. \quad (2.20)$$

³Note that the exact formula (2.16) has not appeared before. In [37], the metric is expanded using some basis functions and their coefficients are related to $l(z_*)$. The advantage of this prescription is to increase the efficiency of numerical computation.

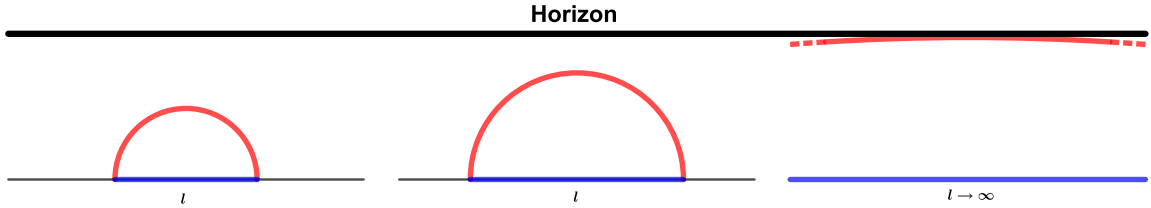


Figure 2. The geodesic probes the deeper spacetime as l increases. As l tends to infinity, the geodesic will approach the horizon.

2.2 Mutual Information

MI is a closely related to EE. It measures the total (both classical and quantum) correlations between two spatial subregions and acts as an upper bound of the connected correlation functions in those regions [53, 59]. The definition of MI between two disjoint subsystems A and B is given by

$$I(A, B) = S_A + S_B - S_{A \cup B}, \quad (2.21)$$

where S_A , S_B and $S_{A \cup B}$ denote the EE of the region A , B and $A \cup B$ respectively with the rest of the system [58]. Note that EE is a divergent quantity, but MI is finite since three divergent parts in eq. (2.21) that depend on the UV cutoff cancel out.

2.2.1 Holographic calculation

Consider two disjoint subsystems with strip regions A and B , each with width l and length $L \rightarrow \infty$. The interval between them is a . For the sake of simplicity, we focus on the symmetric configuration, see figure 3. In this case, $S_{A \cup B} = \min[2S(l), S(2l + a) + S(a)]$. Depending on the ratio a/l , the MI can be written as

$$I(l) = \begin{cases} 2S(l) - S(2l + a) - S(a) & \text{for small ratio } a/l, \\ 0 & \text{for large ratio } a/l. \end{cases} \quad (2.22)$$

For convenience, we will fix a and change l . This induces a critical width l_a below which the MI is zero. Note that one cannot reconstruct anything from the region where MI is zero. In fact, we have not found a way to reconstruct the metric through the MI alone.

2.2.2 Reconstruction method

Here we will propose a method which reconstructs the metric by jointly using EE and MI. Suppose that the field theory data we have are the derivatives of MI and EE with different ranges of l ,⁴

$$I'(l), l > l_a \text{ and } S'(l), l \leq 2l_a + a, \quad (2.23)$$

⁴An interesting question is whether it is possible in reality to know only MI but not EE. MI has some nice properties that EE does not have, such as being finite and non-negative. In view of this, we suspect that in certain situations, it is advantageous to measure the MI directly rather than the EE. At that time, one can know the MI alone.

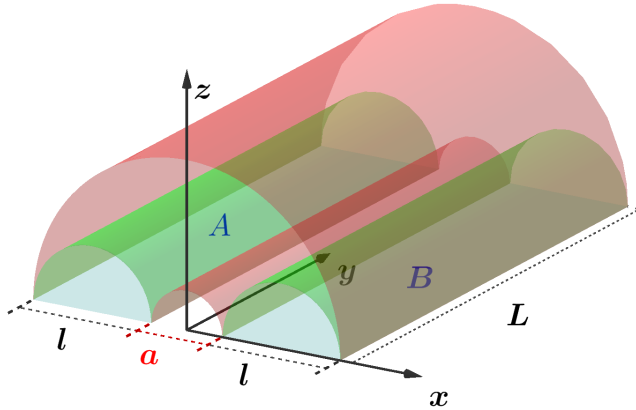


Figure 3. The minimal surfaces (red and green) and two disjoint strip entangling regions (blue) in the symmetric configuration. The nonzero MI is given by the difference between the area of green surfaces and red surfaces.

where a (then l_a) is fixed. A simple but important observation is that one can combine eq. (2.22) and the data (2.23) to iteratively generate $S'(l)$ with any l . The iterative equation can be written as

$$S'(Q) = \begin{cases} S'(Q), & Q \leq Q_a \\ S'\left(\frac{Q-a}{2}\right) - \frac{1}{2}I'\left(\frac{Q-a}{2}\right), & Q_a < Q \leq 2Q_a + a \end{cases} \quad (2.24)$$

where $Q_a = 2l_a + a$. After the n -th iteration, one can generate the data $S'(Q)$ with $Q \leq 2nQ_a + (2n-1)a$. Then the metric can be reconstructed using (2.13) and (2.16).

2.2.3 Example

Let's exhibit our reconstruction method with an example. We still consider $d = 2$ and $f(z) = 1 - z^2$. Using eq. (2.17) and eq. (2.22), we prepare our data as

$$I'(l) = \frac{1}{2} \left[\coth\left(\frac{l}{2}\right) - \coth\left(\frac{a}{2} + l\right) \right], \quad l > l_a \quad (2.25)$$

and

$$S'(l) = \frac{1}{4} \coth\left(\frac{l}{2}\right), \quad l \leq 2l_a + a. \quad (2.26)$$

Here we can specify the critical width

$$l_a = \operatorname{arccosh} \left[\frac{\sqrt{2} \cosh\left(\frac{a}{2}\right) + 5 \cosh(a) - \sqrt{2} \cosh\left(\frac{3a}{2}\right) - 7}{8 \cosh(a) - 10} \right].$$

The associated region where MI is non-zero can be found in figure 4. Note that $Q_a = 2l_a + a$ corresponds to a critical point Z_{*a} in the bulk

$$Z_{*a} = \tanh \left[2 \operatorname{arccoth} \left[(3 - 2\sqrt{2}) \coth\left(\frac{a}{4}\right) \right] \right], \quad (2.27)$$

upon which is the bulk region that cannot be probed by the derivative of EE (2.26) alone. In figure 5, we fix a and plot the change of the relevant geodesics as l increases. In figure 6, we iteratively generate $S'(Q)$ beyond Q_a . In figure 7, we reconstruct the metric.

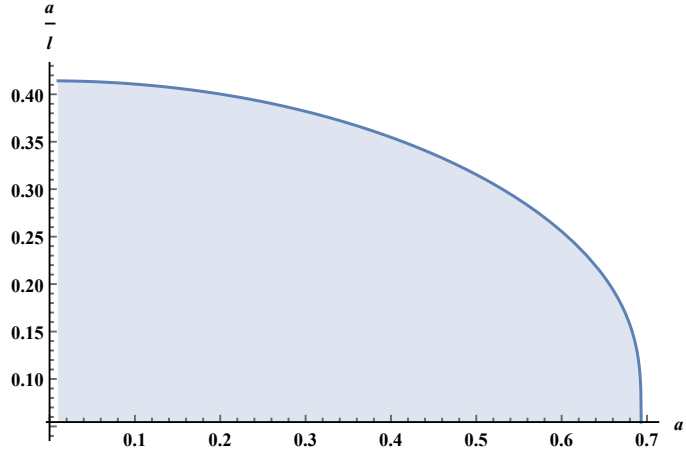


Figure 4. The MI is non-zero only in the blue shaded region.

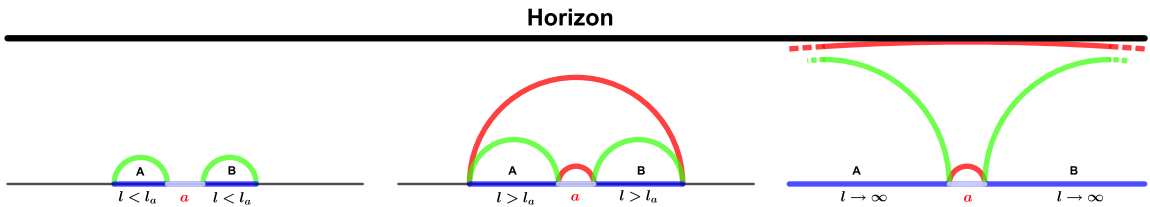


Figure 5. The geodesics relevant to MI vary as l increases. As l tends to infinity, the external red geodesic and two green geodesics approach the horizon in turn.

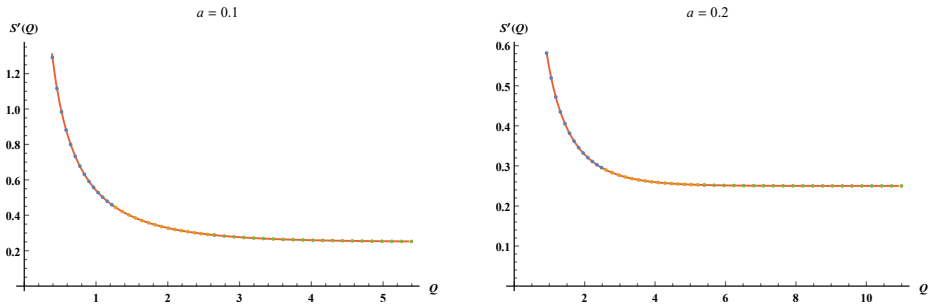


Figure 6. Generate $S'(Q)$ iteratively. Here we set $a = 0.1$ (left) and $a = 0.2$ (right). The solid red line is plotted using the target analytical function. The dotted lines denote the generated function. By three iterations (blue, yellow, green), the domain of $S'(Q)$ expands accordingly.

2.3 Entanglement of Purification

EoP is defined by the minimum EE for all possible purification of the mixed state [54]⁵. It is closely related to MI but is an independent correlation measure [61]. The regularization of EoP has an operational meaning in terms of Einstein-Podolsky-Rosen pairs [54], and it is finite in the CFT [62]. In gravity side it was proposed to be related to the entanglement

⁵Note that a slight generalization of EoP has been used to study the reconstruction of spacelike curves within the entanglement wedge [60].

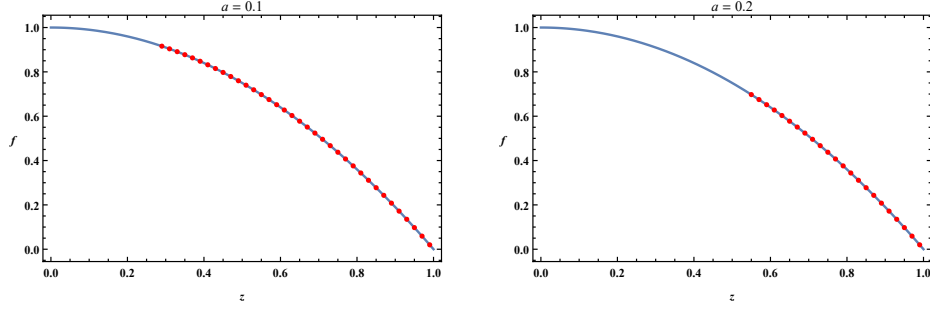


Figure 7. The reconstructed metric over Z_{*a} (red dotted line) using MI and EE. The target metric (blue solid line) is $f = 1 - z^2$. At left and right panels, we set $a = 0.1$ and 0.2 respectively.

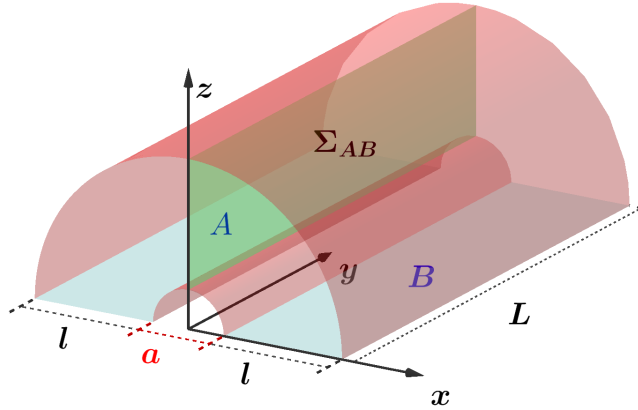


Figure 8. The entanglement wedge with non-zero EoP is a connected region wrapped by the red and blue surfaces. The green surface is the minimum cross section. EoP is determined by its area.

wedge cross section [63, 64]

$$E_W = \min_{\Sigma_{AB}} \left(\frac{Area(\Sigma_{AB})}{4} \right). \quad (2.28)$$

Here A and B represent two disjoint subregions on the boundary. The entanglement wedge is a bulk region surrounded by $AB \equiv A \cup B$ and the minimal surface Γ_{AB} anchored on AB . Σ_{AB} is regarded as a cross section of the entanglement wedge, which divides Γ_{AB} into two parts. E_W can be obtained by minimizing the area of Σ_{AB} over all possible choices of the division.

In figure 8, we plot the geometry for non-zero EoP. We still focus on the symmetric configuration for simplicity. One can find that the EoP is zero when the MI is zero. This is because the entanglement wedge is disconnected and lacks a cross section.

2.3.1 Holographic calculation

Consider the situation with $E_W \neq 0$. The area of Σ_{AB} is

$$A_\Sigma = L^{d-2} \int_{z_*(a)}^{Z_*(Q)} \frac{dz}{\sqrt{f(z)} z^{d-1}}, \quad Q > Q_a, \quad (2.29)$$

where $z_*(a)$ and $Z_*(Q)$ are the turning points of the minimal surfaces with strips of width a and Q , respectively. Using (2.28), we have

$$E_W(Z_*) = \frac{L^{d-2}}{4} \int_{z_*}^{Z_*} \frac{dz}{\sqrt{f(z)}z^{d-1}}, \quad Z_* > Z_{*a}. \quad (2.30)$$

Obviously, it is finite as $z_* > 0$. Take the derivative of eq. (2.30), yielding

$$E'_W(Z_*) = \frac{L^{d-2}}{4} \frac{1}{\sqrt{f(Z_*)}Z_*^{d-1}}, \quad Z_* > Z_{*a}. \quad (2.31)$$

Because this formula is structurally different from eq. (2.11), we cannot use the simple chain rule as before to find the metric-independent mapping $Q \mapsto Z_*$ from the change rate of the EoP with respect to Q .

2.3.2 Reconstruction method

We will propose a numerical method, which include four steps.

1) Discretization

Let's discrete the metric function as $f[z[i]]$, where i denotes an integer in $[0, n]$, $z[i] = i/n$, and n is a large integer. Suppose that the metric $f(z)$ with $z \leq Z_*$ is given, where Z_* belongs to $z[j] \leq Z_* < z[j+1]$ with the integer $j < n$. Build the dataset $\{z[i], f[z[i]]\}$ for any $i \in [0, j]$ and name it as $data_0$.

2) Interpolation

Append a data point $\{z[j+1], f_1\}$ into $data_0$. The value of f_1 will be specified later and the new dataset is named as $data_1$. Interpolate $data_1$ and generate the test metric function $\bar{f}(z)$ which is continuous.

3) Integration

Calculate the numerical integration

$$Q(Z_*) = 2 \int_0^{Z_*} \frac{z^{d-1}}{\sqrt{\bar{f}(z)}\sqrt{Z_*^{2d-2} - z^{2d-2}}} dz, \quad (2.32)$$

$$\bar{E}_W(Z_*) = \frac{L^{d-2}}{4} \int_{z_*}^{Z_*} \frac{dz}{\sqrt{\bar{f}(z)}z^{d-1}}, \quad Z_* > Z_{*a}. \quad (2.33)$$

4) Minimization

Define a loss function

$$\text{loss}(f_1) = |\bar{E}_W(Z_*) - E_W(Q(Z_*))|^2, \quad (2.34)$$

where $E_W(Q)$ is the given data. Substitute eq. (2.32) and eq. (2.33) into eq. (2.34). Minimize the loss function and get the optimal f_1 . After that, set $f[z[j+1]] = f_1$, $j = j+1$, and $data_0 = data_1$.

Finally, iterate the steps 2), 3) and 4). Then the metric with $z > Z_*$ can be reconstructed. Note that this method is characterized by the use of a continuous interpolation function to generate the test metric and thereby we would like to refer it as the interpolation-generated method.

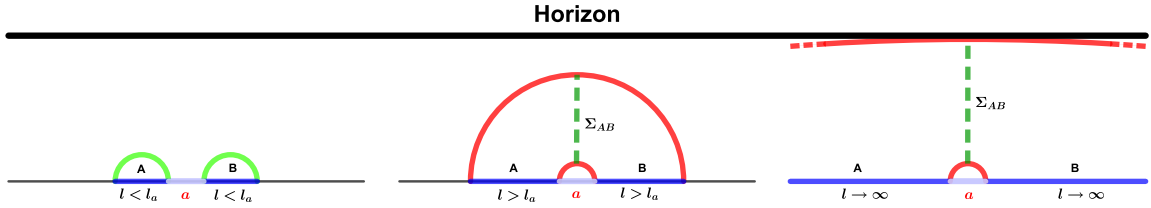


Figure 9. The entanglement wedge and its minimum cross section vary as l increases. As l tends to infinity, the top of the minimum cross section approaches the horizon.

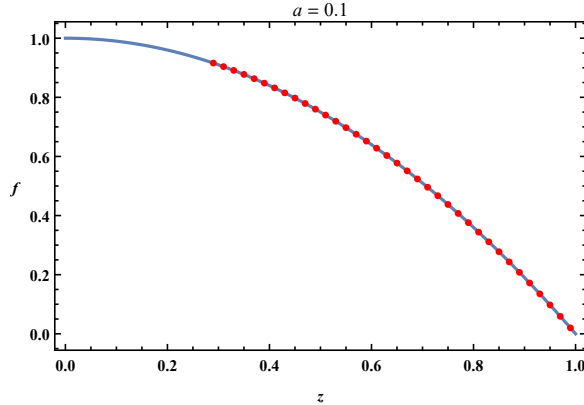


Figure 10. The reconstructed metric over Z_{*a} (red dotted line) using the EoP, provided that the metric below Z_{*a} is given. The target metric (blue solid line) is $f = 1 - z^2$. Here we set $a = 0.1$ and $n = 100$.

2.3.3 Example

For $d = 2$ and $f(z) = 1 - z^2$, the EoP is [65]

$$E_W(Q) = \frac{1}{4} \log \left[\coth \left(\frac{a}{4} \right) \tanh \left(\frac{Q}{4} \right) \right], \quad Q > Q_a, \quad (2.35)$$

which provides us the main data. In addition, we need the metric below Z_{*a} , which can be given by hand or generated by the EE with $Q \leq Q_a$. The rest of the metric can be reconstructed using EoP. In figure 9, we plot the change of the entanglement wedge and minimum cross section as l increases. In figure 10, we show the result of reconstruction⁶, where we have specified $a = 0.1$ and $n = 100$. It is consistent with the left panel of figure 7 as expected.

3 Interior of black holes

Quantum computational complexity is relevant to the number of unitary operators which converts one quantum state to another [66]. In [34], it is found that the interior of a

⁶Using the canned tools in Mathematica (Interpolation, NIntegrate and FindMinimum) with the option WorkingPrecision→30, the reconstruction task can be completed in a few minutes for an average laptop, with a maximum relative error (occurring near the horizon) of 10^{-12} .

black hole can be reconstructed from the complexity, which is defined by ‘complexity = volume’ (CV) proposal [32, 33]. There are other proposals on the holographic complexity, such as ‘complexity = action’ (CA) [67] and ‘complexity = volume 2.0’ (CV2.0) [55]. Recently, a new infinite class of gravitational observables has been proposed to be dual to the complexity [56], which can be referred as ‘complexity = generalized volume’ (CGV). In this section, we will study how to reconstruct the metric in terms of CV2.0 and CGV⁷.

3.1 Complexity = Volume 2.0

The ‘complexity 2.0’ in the gravity side can be expressed as [55]

$$\mathcal{C}_{2.0}(t) = \frac{P}{\hbar} V(t). \quad (3.1)$$

Here, P is the pressure which is related to the cosmological constant $P = -\Lambda/8\pi$ and $V(t)$ is the spacetime volume of the Wheeler-DeWitt (WDW) patch defined in a two-sided eternal AdS black holes. Note that the WDW patch is the domain of dependence of any Cauchy surface in the bulk which is anchored at the time slices on the boundary [67, 68].

3.1.1 Holographic calculation

We first review the calculation of the spacetime volume $V(t)$ under the metric ansatz

$$ds^2 = -f(r)dt^2 + \frac{1}{f(r)}dr^2 + r^2 d\vec{x}^2. \quad (3.2)$$

We consider that the WDW patch moves forward in time in a symmetric way and assume that its two upper null sheets always end at the singularity⁸, see the left panel of figure 11. Using the tortoise coordinate

$$r^*(r) = \int \frac{dr}{f(r)},$$

one can determine the critical time until which the complexity does not increase [69]

$$t_c = 2(r^*(\infty) - r^*(r_s)), \quad (3.3)$$

where r_s denotes the position of singularity. To calculate the spacetime volume, we divide the WDW patch into several parts. Due to the symmetric configuration, we just need to calculate the volumes of three regions which are labeled in the right panel of figure 11. Using the integration formula of the spacetime volume

$$V = \int_{WDW} d^{d+1}x \sqrt{-g} = \Sigma_{d-1} \int dt dr r^{d-1} \quad (3.4)$$

where Σ_{d-1} denotes the regulated volume of the $d-1$ spatial boundary directions, we have

$$V_1 = \Sigma_{d-1} \int_{r_s}^{r_h} dr r^{d-1} (t_R + r^*(\infty) - r^*(r)), \quad (3.5)$$

⁷We do not know how to reconstruct using the CA proposal. Note that we cannot specify the action that serves as a metric functional. Otherwise the metric can be obtained through the variation. We suspect that such a reconstruction method is highly non-trivial, if existed.

⁸This holds for a class of black holes which have the Penrose diagrams with similar structures.

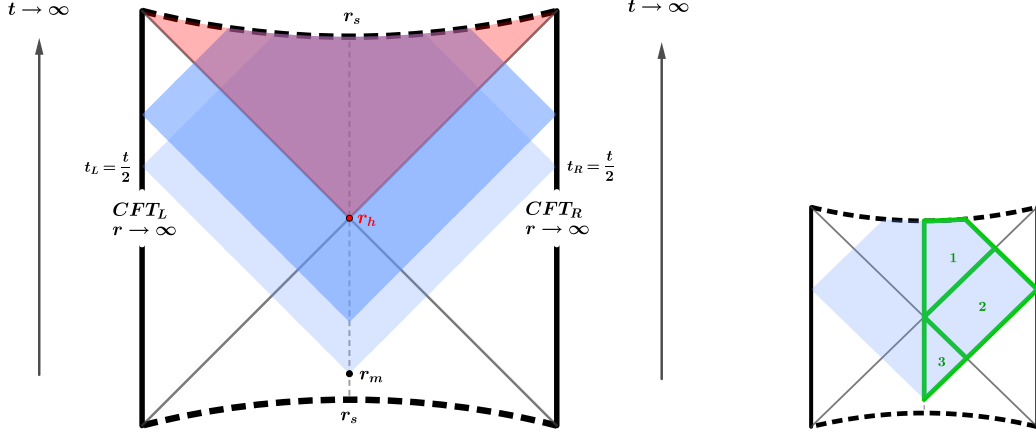


Figure 11. Left: The time evolution of the WDW patch in a two-sided AdS black hole. It is anchored at two boundary time slices $t_L = t/2$ and $t_R = t/2$. Two lower null sheets intersect at point r_m and two upper null sheets end at the singularity r_s . As time grows, the WDW patch moves upward, through three shaded areas. The intersection r_m will eventually approach the horizon r_h . Right: Three typical blocks of the WDW patch are labeled for the calculation of its volume.

$$V_2 = 2\Sigma_{d-1} \int_{r_h}^{r_{uv}} dr r^{d-1} (r^*(\infty) - r^*(r)), \quad (3.6)$$

$$V_3 = \Sigma_{d-1} \int_{r_m}^{r_h} dr r^{d-1} (-t_R + r^*(\infty) - r^*(r)), \quad (3.7)$$

where r_m is determined by

$$t - t_c = 2(r^*(r_s) - r^*(r_m)) \quad (3.8)$$

and r_{uv} is the UV cutoff. As a result, one can see [70]

$$\frac{dV}{dt} = \frac{\Sigma_{d-1}}{d} (r_m^d - r_s^d). \quad (3.9)$$

By setting $\delta t = t - t_c$ and $r_s = 0$, we rewrite eq. (3.9) and eq. (3.8) as

$$\mathcal{C}'_{2,0}(\delta t) = \frac{P}{\hbar} \frac{\Sigma_{d-1}}{d} r_m^d, \quad (3.10)$$

$$\delta t = -2 \int_0^{r_m} \frac{dr}{f(r)}. \quad (3.11)$$

3.1.2 Reconstruction method

Our data is $\mathcal{C}'_{2,0}(\delta t)$ of the boundary field theory. Inputting the data into eq. (3.10), we can calculate the derivative $\delta t'(r_m)$. Taking the derivative on both sides of eq. (3.11), we obtain a very simple formula to reconstruct the metric inside the horizon

$$f(r_m) = -\frac{2}{\delta t'(r_m)}. \quad (3.12)$$

In ref. [34], the reconstruction of the interior of black holes requires information from the exterior. Here, we have shown that this is not necessary as soon as we update the proposal from CV to CV2.0.

3.1.3 Example

Suppose $f(r) = r^2 - 1$ and $d = 2$. Calculating eq. (3.11) and taking the inverse, we find

$$r_m = \tanh\left(\frac{\delta t}{2}\right). \quad (3.13)$$

Inserting it into (3.10), we read the complexity growth

$$C'_{2,0}(\delta t) = \frac{P}{\hbar} \frac{\Sigma_1}{2} \tanh^2\left(\frac{\delta t}{2}\right). \quad (3.14)$$

With the data (3.14) in hand, we solve eq. (3.10) to give⁹

$$\delta t(r_m) = 2 \operatorname{arctanh}(r_m). \quad (3.15)$$

Using the reconstruction formula (3.12), we obtain the metric finally

$$f(r_m) = r_m^2 - 1. \quad (3.16)$$

3.2 Complexity = Generalized Volume

Recently, the CV proposal has been generalized in [56]. It is presented that the holographic dual of quantum complexity may be expressed as an integral of a scalar functional F_1 , which depends on the background metric $g_{\mu\nu}$ and the embedding $X^\mu(\sigma^a)$ of the codimension-one hypersurface Σ_{F_2} . The hypersurface Σ_{F_2} is anchored on the time slice Σ_t of the boundary and is determined by extremizing another functional F_2 . In general, F_1 is different from F_2 . For the simple case $F_1 = F_2$, the generalized volume can be written as

$$C_{gen}(t) = \max_{\partial\Sigma=\Sigma_t} \left[\frac{1}{L} \int_{\Sigma(t)} d^d\sigma \sqrt{h} F_1(g_{\mu\nu}, X^\mu) \right], \quad (3.17)$$

where L is the AdS radius and h is the determinant of induced metric. Here we will explore the reconstruction using eq. (3.17), provided F_1 depends only on the curvature invariant

$$F_1 = 1 + \mathcal{K} L^4 C^2,$$

where $C^2 \equiv C_{\mu\nu\rho\sigma} C^{\mu\nu\rho\sigma}$ denotes the square of the Weyl tensor for the bulk spacetime and \mathcal{K} is the coupling constant [56].

3.2.1 Holographic calculation

Let's write the line element in the Eddington-Finkelstein coordinates

$$ds^2 = -f(r)dv^2 + 2dvdr + r^2 d\vec{x}^2, \quad (3.18)$$

where $v = t + r^*(r)$. By describing the extremal hypersurface by the parametric equations $v(\sigma)$ and $r(\sigma)$, the generalized volume can be rewritten in a specific form [56]

$$C_{gen} = \int_{\Sigma} d\sigma r^{d-1} \sqrt{-f(r)\dot{v}^2 + 2\dot{v}\dot{r}a(r)}. \quad (3.19)$$

⁹Interestingly, this boundary-bulk relation encoded in CV2.0 has the same form as the one encoded in EE, see eq. (2.19).

Here we have set $L = 1$ and $a(r)$ is a factor about the curvature, given by

$$a(r) = 1 + \mathcal{K} \frac{d-2}{d} \frac{1}{r^4} [2f(r) + r(rf''(r) - 2f'(r))]^2. \quad (3.20)$$

We can express the generalized volume \mathcal{C}_{gen} and the boundary time t in terms of the metric $f(r)$ and the minimal radius r_{min} of the surface

$$\mathcal{C}_{gen} = -2\Sigma_{d-1} \int_{r_{min}}^{r_{uv}} \frac{U(r)}{f(r)\sqrt{U(r_{min}) - U(r)}} dr, \quad (3.21)$$

$$t = -2 \int_{r_{min}}^{\infty} \frac{\sqrt{U(r_{min})}}{f(r)\sqrt{U(r_{min}) - U(r)}} dr, \quad (3.22)$$

where $U(r) = -f(r) a^2(r) r^{2(d-1)}$ can be understood as an effective potential of a classical particle [56]. In order to cancel r_{min} in two equations above, we take derivatives:

$$\frac{d\mathcal{C}_{gen}}{dr_{min}} = 2\Sigma_{d-1} \left\{ \int_{r_{min}}^{\infty} \frac{U(r)U'(r_{min})}{2f(r)[U(r_{min}) - U(r)]^{\frac{3}{2}}} + \frac{U(r_{min})}{\sqrt{f(r_{min})}} \lim_{r \rightarrow r_{min}} \frac{1}{\sqrt{U(r_{min}) - U(r)}} \right\}, \quad (3.23)$$

$$\frac{dt}{dr_{min}} = \frac{2}{\sqrt{U(r_{min})}} \left\{ \int_{r_{min}}^{\infty} \frac{U(r)U'(r_{min})}{2f(r)[U(r_{min}) - U(r)]^{\frac{3}{2}}} + \frac{U(r_{min})}{\sqrt{f(r_{min})}} \lim_{r \rightarrow r_{min}} \frac{1}{\sqrt{U(r_{min}) - U(r)}} \right\}. \quad (3.24)$$

Using the chain rule, the time derivative of the generalized volume is given by

$$\frac{d\mathcal{C}_{gen}}{dt} = \Sigma_{d-1} \sqrt{U(r_{min})}. \quad (3.25)$$

As $t \rightarrow \infty$, this asymptotically approaches a constant

$$\frac{d\mathcal{C}_{gen}}{dt} = \lim_{t \rightarrow \infty} \Sigma_{d-1} \sqrt{U(r_{min})} = \Sigma_{d-1} \sqrt{U(r_f)}, \quad (3.26)$$

where $r = r_f$ is the radius of the locally maximal effective potential. Note that in the whole time evolution, we assume that the maximal extremal hypersurface changes continuously, without any sudden jumps [34].

3.2.2 Reconstruction method

Setting $\omega = r^d$, we rewrite (3.22) and (3.25) as

$$t = -\frac{2}{d} \int_{\omega_{min}}^{\infty} \frac{\sqrt{U(\omega_{min})} \omega^{\frac{1}{d}-1}}{f(\omega)\sqrt{U(\omega_{min}) - U(\omega)}} d\omega, \quad (3.27)$$

$$\frac{d\mathcal{C}_{gen}}{dt} = \Sigma_{d-1} \sqrt{U(\omega_{min})}, \quad (3.28)$$

where

$$U(\omega) = -f(\omega) a^2(\omega) \omega^{2(1-\frac{1}{d})}, \quad (3.29)$$

and

$$a(\omega) = 1 + \mathcal{K} \frac{d-2}{d} \frac{1}{\omega^{\frac{4}{d}}} \{2f(\omega) + \omega d [\omega d f''(\omega) + (d-3)f'(\omega)]\}. \quad (3.30)$$

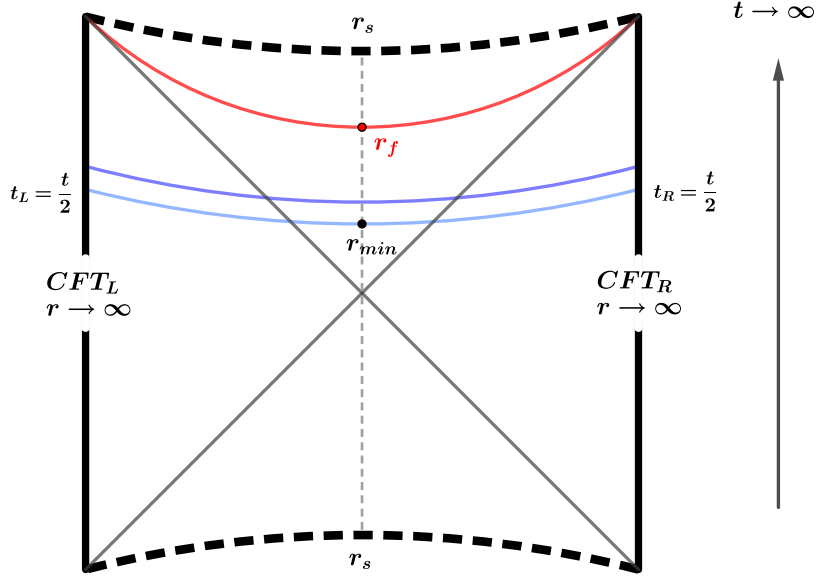


Figure 12. The time evolution of the extremal hypersurface in a two-sided AdS black hole. As time grows, the hypersurface moves up. The two nearby blue curves correspond to the hypersurfaces anchored at two adjacent times. As time tends to infinity, the hypersurface with minimal radius r_{min} approaches to the one with r_f (red curve), at which an effective potential is locally maximal.

To proceed, we assume that $U(\omega)$ is monotonic from ω_{min} to ∞ . Then $U = U(\omega)$ can be inverted to a single-valued function $\omega = \omega(U)$. This allows us to change (3.27) as

$$\frac{t(U_{min})}{\sqrt{U_{min}}} = \int_{U_{min}}^{-\infty} \frac{y(U)}{\sqrt{U_{min} - U}} dU, \quad (3.31)$$

where we have defined a function

$$y(U) = \frac{2}{d} \frac{a^2(\omega) \omega^{1-\frac{1}{d}} d\omega}{U}. \quad (3.32)$$

One can interpret (3.31) as the Cauchy principal value to deal with the integrand of (3.27) which blows up near the horizon ω_h . Concretely, we rewrite (3.31) as

$$\frac{t(U_{min})}{\sqrt{U_{min}}} = \left(\int_{U_{min}}^{\epsilon} + \int_{\epsilon}^{-\epsilon} + \int_{-\epsilon}^{-\infty} \right) \frac{y(U)}{\sqrt{U_{min} - U}} dU, \quad (3.33)$$

where $U_{min} = U(\omega_{min})$. We assume that ϵ is small enough that the second integral $\int_{\epsilon}^{-\epsilon}$ cancels by itself. Then we have

$$\frac{t(U_{min})}{\sqrt{U_{min}}} = \left(\int_{U_{min}}^{\epsilon} + \int_{-\infty}^{-\epsilon} \right) \frac{y(U)}{\sqrt{U_{min} - U}} dU, \quad (3.34)$$

which can be further recast as

$$W(U_{min}) \equiv -\frac{t(U_{min})}{\sqrt{U_{min}}} - \int_{-\infty}^{-\epsilon} \frac{y(U)}{\sqrt{U_{min} - U}} dU = \int_{\epsilon}^{U_{min}} \frac{y(U)}{\sqrt{U_{min} - U}} dU. \quad (3.35)$$

Using eq. (2.14), the above integral equation can be solved

$$y(U) = \frac{1}{\pi} \frac{d}{dU} \int_{\epsilon}^U \frac{W(U_{min})}{\sqrt{U - U_{min}}} dU_{min}. \quad (3.36)$$

Combining eq. (3.32), we find

$$\frac{2}{d} \frac{a^2(\omega)}{U} \omega^{1-\frac{1}{d}} \frac{d\omega}{dU} = \frac{1}{\pi} \frac{d}{dU} \int_{\epsilon}^U \frac{W(U_{min})}{\sqrt{U - U_{min}}} dU_{min}. \quad (3.37)$$

Some remarks are in order. Firstly, our main data is the derivative of the generalized volume. Using eq. (3.28), one can calculate the function $t(U_{min})$. In addition, we assume that the metric outside the horizon is given. As a result, we can obtain the function $W(U_{min})$. Secondly, consider the CV proposal where the factor $a = 1$. One can see that eq. (3.37) is reduced to a first-order ordinary differential equation (ODE) of the function $\omega(U)$. Solving the ODE and using eq. (3.29), the metric $f(\omega)$ can be reconstructed [34]. Thirdly, for a general factor, we can insert eq. (3.29) and eq. (3.30) into eq. (3.37), which is changed into a complex third-order ODE of the metric function. Fortunately, it still can be solved by the canned differential equation solvers such as Mathematica’s NDSolve with the method option “EquationSimplification” \rightarrow “Residual” [71].

3.2.3 Example

Consider the AdS black hole with the target metric $f(\omega) = (\omega - 1)\omega^{\frac{2}{d}-1}$. We read the factor (3.30) and the potential (3.29) as

$$a(\omega) = 1 + \kappa \left(\frac{1}{\omega} \right)^2, \quad (3.38)$$

$$U(\omega) = -\frac{(\omega - 1)(\omega^2 + \kappa)^2}{\omega^3}, \quad (3.39)$$

where $\kappa = d(d-1)^2(d-2)\mathcal{K}$. By analyzing the function (3.39), it has been pointed out that there is one local maximum inside the horizon when $-1 < \kappa < \kappa_1 = \frac{1}{8}(47 - 13\sqrt{13}) \approx 0.016$ [56], see figure 13. Note that the existence of at least one local maximum inside the horizon is the requirement for the linear growth of the generalized volume. In the following, we will focus on the cases with $d = 3$ and $\kappa = -0.5, 0.01$. Using the target metric, we generate the data $C'_{gen}(t)$ and the function $W(U_{min})$ we need¹⁰, see figures 14 and 15. Solving the third-order ODE mentioned above with the boundary condition given by the target metric near the horizon, we reconstruct the metric inside the horizon, see figure 16. One can find that we build the metric within (ω_f, ω_h) where ω_f depends on κ . In general, it is not possible to probe the singularity at ω_s if $\omega_f > \omega_s$.

4 Comparison

Our work is closely related to refs. [15, 24, 34], where the metric reconstruction has been studied using three measures: EE, WL and CV. Now we have extended their work to MI,

¹⁰We specify the small quantity in eq. (3.35) as $\epsilon = 10^{-9}$.

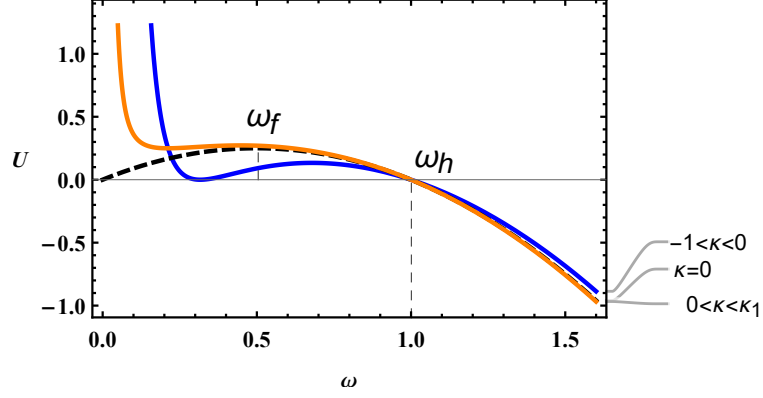


Figure 13. The effective potential $U(\omega)$ with $-1 < \kappa < \kappa_1$ has the extremal point located at ω_f which is within the horizon located at $\omega_h = 1$. $U(\omega)$ is monotonic from ω_f to ∞ .

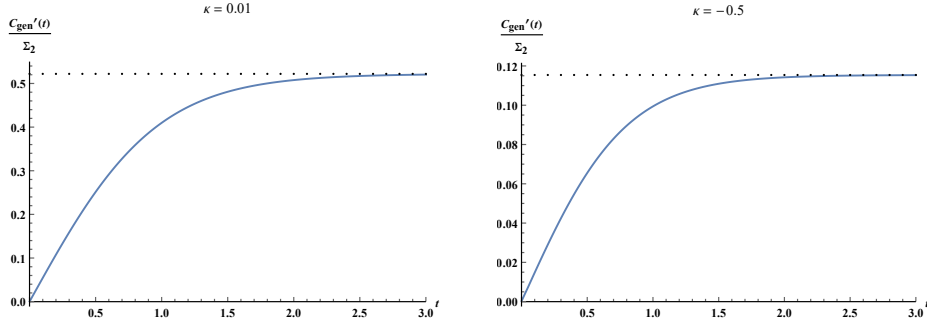


Figure 14. The change rate of generalized volume (blue solid line). At the late time, it will hit the gray dotted line, which can be described by eq. (3.26). The left and right correspond to $\kappa = 0.01$ and $\kappa = -0.5$ respectively.

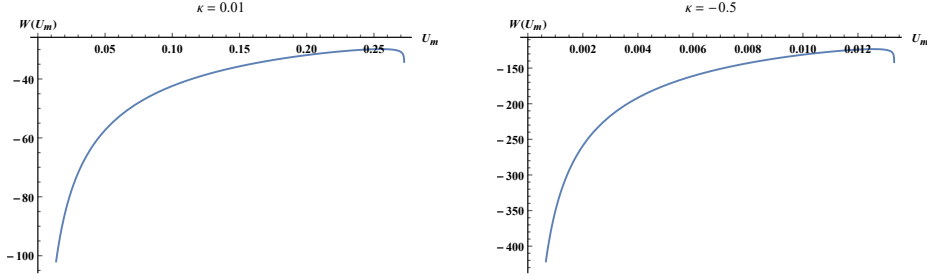


Figure 15. The function $W(U_{min})$ that is required for the reconstruction.

EoP, CV2.0 and CGV. In table 1, we compare these seven reconstruction methods from six aspects.

- 1) Is the measure sensitive or insensitive to UV cutoff?
- 2) Is the change rate of the measure sensitive or insensitive to UV cutoff?
- 3) Is the measure sufficient or insufficient to reconstruct the metric?
- 4) Does the measure probe the exterior or interior of a black hole?
- 5) Does the measure depend on the spatial or temporal boundary scale?

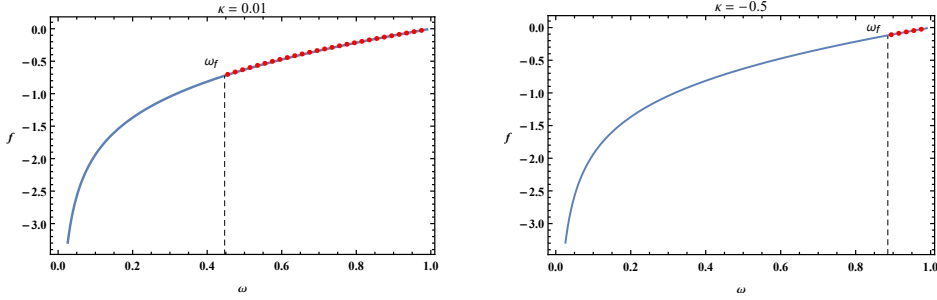


Figure 16. The reconstructed metric (red dotted line) using the generalized volume. The blue solid line is the target metric. The region deeper than ω_f cannot be probed.

6) Does the measure probe the spacetime in a local or non-local way?

Property	1	2	3	4	5	6
EE	Sensitive	Insensitive	Sufficient	Exterior	Spatial	Local
WL	Sensitive	Insensitive	Sufficient	Exterior	Spatial	Local
MI	Insensitive	Insensitive	Insufficient	Exterior	Spatial	Local
EoP	Insensitive	Insensitive	Insufficient	Exterior	Spatial	Local
CV	Sensitive	Insensitive	Insufficient	Interior	Temporal	Local
CV2.0	Sensitive	Insensitive	Sufficient	Interior	Temporal	Local
CGV	Sensitive	Insensitive	Insufficient	Interior	Temporal	Local

Table 1. Comparison of reconstruction methods using seven measures across six properties.

Some remarks on the comparison are in order.

i) Most of measures are sensitive to UV cutoff but their derivatives are not.

ii) For EE, WL, and CV2.0, each of them is sufficient to reconstruct the metric, given some assumptions about spacetime symmetry and structure. For other measures, the metric (or equivalent information) must be given for part of the spacetime.

iii) The measures related to the EE with spatial scales probe the exterior of black holes, while the measures related to the complexity with temporal scales probe the interior. This reflects the complementary nature of spatial entanglement and time-evolved complexity in encoding spacetime.

iv) All these measures probe the spacetime in a local way: reconstructing the metric in different radial positions requires the information at different boundary scales¹¹.

In order to better understand the last point, we will review briefly the reconstruction method by the DL from shear-viscosity data [43]. One can find that the holographic renormalization group flow of the shear viscosity is described by the first-order ODE [43]

$$\left(\eta - \frac{i\omega}{f}\right)' + \frac{i\omega}{f} \left[z^2 \left(\eta - \frac{i\omega}{z}\right)^2 - \frac{1}{z^2} \right] = 0, \quad (4.1)$$

¹¹Note that the meaning of local way defined here is slightly different from that given in [43].

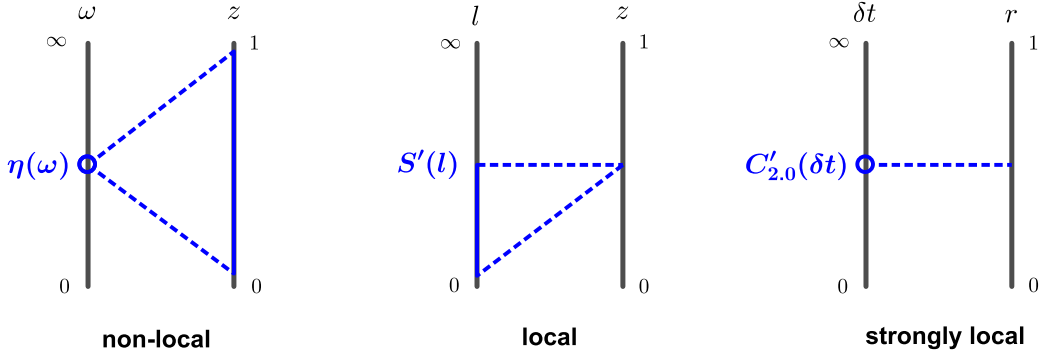


Figure 17. Three typical ways to probe the spacetime that can be described as non-local, local and strongly local, respectively. Left: The complete metric from $z = 0$ to $z = 1$ can be learned from the data $\eta(\omega)$ with narrow frequency range. Middle: To build the metric $f(z)$ at a given z , the data $S'(l)$ with a finite range $(0, l]$ is required. Right: The metric $f(r)$ at a given r can be built from the data $C'_{2,0}(\delta t)$ around the corresponding δt .

where the metric ansatz (2.2) has been used. Given the metric $f(z)$ and the regular condition at horizon $\eta(\omega, 1) = 1 + i\omega$, the ODE can be solved to yield $\eta(\omega, 0)$, which is the frequency-dependent shear viscosity on the boundary field theory. In ref. [43], a discretized representation of the ODE (4.1) is provided through a deep neural network, where the metric is encoded as trainable weights. Given the existence of the horizon and guided by the smoothness of spacetime, it is shown that three typical black hole metrics can be extracted with high accuracy from $\eta(\omega, 0)$ using DL. In particular, the deep neural network exhibits an excellent generalization ability, indicating that the complete metric can be well learned from the data with narrow frequency range.

We can classify all the reconstruction methods mentioned above into three types, the basis of which can be seen in figure 17 and explained below. The first is shear viscosity, which is characterised by the excellent generalization ability and can be understood intuitively as follows. Looking at eq. (4.1), one can find that in order to determine $\eta(\omega, 0)$ at any non-zero frequency, the complete metric from $z = 0$ to $z = 1$ must be known. Conversely, each $\eta(\omega, 0)$ at a non-zero frequency contains some information about the metric at any z . Therefore, if the technique of information mining is powerful enough, it is in principle possible to reconstruct the complete metric from a narrow frequency range, at least when the metric function is simple enough. The second involves EE, WL, MI, EoP, CV and CGV. Taking EE as an example, two equations (2.13) and (2.16) show that if we want to probe deeper into spacetime¹², we need data $S'(l)$ at larger l . In addition, to build $f(z)$ at a given z , the data $S'(l)$ with a finite range $(0, l]$ is required. The third is CV2.0. From (3.10)-(3.12) and the left panel of figure 11, we know that it probes the shallower spacetime as the data $C'_{2,0}(\delta t)$ with larger δt is input. Moreover, one can reconstruct the metric $f(r)$ at certain r *if and only if* a small range of data $C'_{2,0}(\delta t)$ around the corresponding δt is provided, see figure 18. We therefore argue that the reconstruction method using

¹²We consider that the horizon is deeper than the boundary but shallower than the singularity.

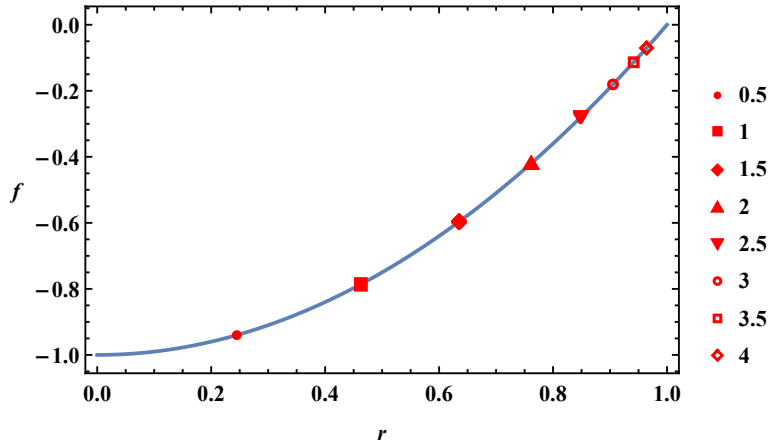


Figure 18. The bulk metric reconstruction with strong locality. The red labels denote the reconstruction results using the data $\mathcal{C}'_{2,0}(\delta t)$ around given δt . The blue solid line is the target metric. We choose eight δt which are listed on the right. The small ranges around them are fixed as $[\delta t - 0.1\delta t, \delta t + 0.1\delta t]$. Within each small range, we take a uniform sample of 100 points as our data.

CV2.0 has a certain strong locality¹³. Despite its distinctiveness, CV2.0 still shares some commonality with the second type: reconstructing metrics of different radial positions always requires the data of different boundary scales. Note that here the measures can be relevant to entanglement or complexity, and the boundary scale can be either spatial or temporal.

5 Summary

Following the spirit of ‘It from Qubit’ [76], we investigate the bulk reconstruction of black hole metrics using various quantum information measures on the boundary field theories. We propose several reconstruction methods all of which are free of UV divergence. One can see that different mathematical ingredient appears in each method: analytic formulas for EE, iterative data generation for MI, interpolation-generated test metrics for EoP, simple derivatives for CV2.0, and a complex three-order ODE for CGV. We also witness the complementarity of entanglement and complexity, and analyse the differences and similarities among different probing ways¹⁴. Our results would enrich the understanding of how field theory encodes gravity.

In the future, it would be important to reduce the assumptions of the reconstruction methods and thus broaden their applicability. In this regard, one can draw lessons from the bulk reconstruction that do not rely on spacetime symmetries [77, 78], as well as the illumination on entanglement shadows [79–81]. Meanwhile, one can collect experimental

¹³Here the strong locality can be understood as a property of the mapping between the boundary data and the bulk radial metric. In figure 17, three types of mappings have been visualized. Their properties should not be confused with those of the boundary quantities themselves. For example, the complexity on the boundary is defined over the entire time slice and therefore it is highly non-local.

¹⁴Our analysis is limited to the current settings. For example, we focus on the simple strip entangling region and do not consider other shapes.

and simulated data on quantum information measures in strongly coupled field theories with gravity duals. It would be intriguing to explore whether the reconstruction methods can extract reasonable holographic spacetimes from these data¹⁵.

Acknowledgments

We thank Xian-Hui Ge, Yu Tian and Run-Qiu Yang for helpful discussions. This work was supported partially by NSFC grants (No.11675097).

References

- [1] J.M. Maldacena, *The Large N limit of superconformal field theories and supergravity*, *Adv. Theor. Math. Phys.* **2** (1998) 231 [[hep-th/9711200](#)].
- [2] S.S. Gubser, I.R. Klebanov and A.M. Polyakov, *Gauge theory correlators from noncritical string theory*, *Phys. Lett. B* **428** (1998) 105 [[hep-th/9802109](#)].
- [3] E. Witten, *Anti-de Sitter space and holography*, *Adv. Theor. Math. Phys.* **2** (1998) 253 [[hep-th/9802150](#)].
- [4] L. Susskind and E. Witten, *The Holographic bound in anti-de Sitter space*, (1998) [[hep-th/9805114](#)].
- [5] H. Liu and J. Sonner, *Quantum many-body physics from a gravitational lens*, *Nature Rev. Phys.* **2** (2020) 615 [[arXiv:2004.06159](#)].
- [6] A. Hamilton, D.N. Kabat, G. Lifschytz and D.A. Lowe, *Holographic representation of local bulk operators*, *Phys. Rev. D* **74** (2006) 066009 [[hep-th/0606141](#)].
- [7] T. De Jonckheere, *Modave lectures on bulk reconstruction in AdS/CFT*, *PoS Modave2017* (2018) 005 [[arXiv:1711.07787](#)].
- [8] D. Harlow, *TASI Lectures on the emergence of bulk physics in AdS/CFT*, *PoS TASI2017* (2018) 002 [[arXiv:1802.01040](#)].
- [9] N. Kajuri, *Lectures on bulk reconstruction*, *SciPost Phys. Lect. Notes* **22** (2021) [[arXiv:2003.00587](#)].
- [10] S. de Haro, S.N. Solodukhin and K. Skenderis, *Holographic reconstruction of space-time and renormalization in the AdS / CFT correspondence*, *Commun. Math. Phys.* **217** (2001) 595 [[hep-th/0002230](#)].
- [11] J. Hammersley, *Extracting the bulk metric from boundary information in asymptotically AdS spacetimes* *JHEP* **12** (2006) 047 [[hep-th/0609202](#)].
- [12] V.E. Hubeny, H. Liu and M. Rangamani, *Bulk-cone singularities & signatures of horizon formation in AdS/CFT* *JHEP* **01** (2007) 009 [[hep-th/0610041](#)].
- [13] J. Hammersley, *Numerical metric extraction in AdS/CFT*, *Gen. Rel. Grav.* **40** (2008) 1619 [[arXiv:0705.0159](#)].
- [14] S. Bilson, *Extracting spacetimes using the AdS/CFT conjecture*, *JHEP* **08** (2008) 073 [[arXiv:0807.3695](#)].

¹⁵After this work was completed, we are aware of an exciting recent progress [82], where the holographic bulk metrics are reconstructed from the derivative of EE in the lattice Yang-Mills theory.

- [15] S. Bilson, *Extracting Spacetimes using the AdS/CFT Conjecture: Part II*, *JHEP* **02** (2011) 050 [[arXiv:1012.1812](#)].
- [16] V.E. Hubeny, *Extremal surfaces as bulk probes in AdS/CFT*, *JHEP* **07** (2012) 093 [[arXiv:1203.1044](#)].
- [17] V. Balasubramanian, B.D. Chowdhury, B. Czech, J. de Boer and M.P. Heller, *Bulk curves from boundary data in holography*, *Phys. Rev. D* **89** (2014) 086004 [[arXiv:1310.4204](#)].
- [18] R.C. Myers, J. Rao and S. Sugishita, *Holographic Holes in Higher Dimensions*, *JHEP* **06** (2014) 044 [[arXiv:1403.3416](#)].
- [19] B. Czech and L. Lamprou, *Holographic definition of points and distances*, *Phys. Rev. D* **90** (2014) 106005 [[arXiv:1409.4473](#)].
- [20] N. Engelhardt and G.T. Horowitz, *Towards a Reconstruction of General Bulk Metrics*, *Class. Quant. Grav.* **34** (2017) 015004 [[arXiv:1605.01070](#)].
- [21] N. Engelhardt and G.T. Horowitz, *Recovering the spacetime metric from a holographic dual*, *Adv. Theor. Math. Phys.* **21** (2017) 1635 [[arXiv:1612.00391](#)].
- [22] S.R. Roy and D. Sarkar, *Bulk metric reconstruction from boundary entanglement*, *Phys. Rev. D* **98** (2018) 066017 [[arXiv:1801.07280](#)].
- [23] D. Kabat and G. Lifschytz, *Emergence of spacetime from the algebra of total modular Hamiltonians*, *JHEP* **05** (2019) 017 [[arXiv:1812.02915](#)].
- [24] K. Hashimoto, *Building bulk from Wilson loops*, *PTEP* **2021** (2021) 023B04 [[arXiv:2008.10883](#)].
- [25] S. Caron-Huot, *Holographic cameras: An eye for the bulk*, *JHEP* **03** (2023) 047 [[arXiv:2211.11791](#)].
- [26] J.M. Maldacena, *Eternal black holes in anti-de Sitter*, *JHEP* **04** (2003) 021 [[hep-th/0106112](#)].
- [27] S. Ryu and T. Takayanagi, *Holographic derivation of entanglement entropy from AdS/CFT*, *Phys. Rev. Lett.* **96** (2006) 181602 [[hep-th/0603001](#)].
- [28] M. Van Raamsdonk, *Building up spacetime with quantum entanglement*, *Gen. Rel. Grav.* **42** (2010) 2323 [[arXiv:1005.3035](#)].
- [29] B. Swingle, *Entanglement Renormalization and Holography*, *Phys. Rev. D* **86** (2012) 065007 [[arXiv:0905.1317](#)].
- [30] J. Maldacena and L. Susskind, *Cool horizons for entangled black holes*, *Fortsch. Phys.* **61** (2013) 781 [[arXiv:1306.0533](#)].
- [31] M. Rangamani, T. Takayanagi, *Aspects of Holographic Entanglement Entropy*, *JHEP* **08** (2018) 045 [[hep-th/0605073](#)].
- [32] L. Susskind, *Entanglement is not enough*, *Fortsch. Phys.* **64** (2016) 49 [[arXiv:1411.0690](#)].
- [33] L. Susskind, *Computational Complexity and Black Hole Horizons*, *Fortsch. Phys.* **64** (2016) 24 [[arXiv:1403.5695](#)].
- [34] K. Hashimoto and R. Watanabe, *Bulk reconstruction of metrics inside black holes by complexity*, *JHEP* **09** (2021) 165 [[arXiv:2103.13186](#)].
- [35] K. Skenderis, *Lecture notes on holographic renormalization*, *Class. Quantum. Gravity* **19** (2002) 5849 [[hep-th/0209067](#)].

- [36] I. Papadimitriou, *Lectures on Holographic Renormalization, Springer Proceedings in Physics Vol. 176: Theoretical Frontiers in Black Holes and Cosmology*, Springer Press (2016).
- [37] N. Jokela and A. Pönni, *Towards precision holography*, *Phys. Rev. D* **103** (2021) 026010 [[arXiv:2007.00010](#)].
- [38] K. Hashimoto, S. Sugishita, A. Tanaka and A. Tomiya, *Deep learning and the AdS/CFT correspondence*, *Phys. Rev. D* **98** (2018) 046019 [[arXiv:1802.08313](#)].
- [39] K. Hashimoto, S. Sugishita, A. Tanaka and A. Tomiya, *Deep Learning and Holographic QCD*, *Phys. Rev. D* **98** (2018) 106014 [[arXiv:1809.10536](#)].
- [40] K. Hashimoto, *AdS/CFT correspondence as a deep Boltzmann machine*, *Phys. Rev. D* **99** (2019) 106017 [[arXiv:1903.04951](#)].
- [41] J. Tan and C.B. Chen, *Deep learning the holographic black hole with charge*, *Int. J. Mod. Phys. D* **28** (2019) 1950153 [[arXiv:1908.01470](#)].
- [42] T. Akutagawa, K. Hashimoto and T. Sumimoto, *Deep Learning and AdS/QCD*, *Phys. Rev. D* **102** (2020) 026020 [[arXiv:2005.02636](#)].
- [43] Y.K. Yan, S.F. Wu, X.H. Ge and Y. Tian, *Deep learning black hole metrics from shear viscosity*, *Phys. Rev. D* **102** (2020) 101902(R) [[arXiv:2004.12112](#)].
- [44] K. Hashimoto, H.Y. Hu and Y.Z. You, *Neural ordinary differential equation and holographic quantum chromodynamics*, *Mach. Learn. Sci. Tech.* **2** (2021) 035011 [[arXiv:2006.00712](#)].
- [45] K. Hashimoto, K. Ohashi and T. Sumimoto, *Deriving the dilaton potential in improved holographic QCD from the meson spectrum*, *Phys. Rev. D* **105** (2022) 106008 [[arXiv:2108.08091](#)].
- [46] R. Katsube, W.H. Tam, M. Hotta and Y. Nambu, *Deep learning metric detectors in general relativity*, *Phys. Rev. D* **106** (2022) 044051 [[arXiv:2206.03006](#)].
- [47] K. Hashimoto, K. Ohashi and T. Sumimoto, *Deriving dilaton potential in improved holographic QCD from chiral condensate*, *PTEP* **2023** (2023) 033B01 [[arXiv:2209.04638](#)].
- [48] K. Li, Y. Ling, P. Liu and M.H. Wu, *Learning the black hole metric from holographic conductivity*, *Phys. Rev. D* **107** (2023) 066021 [[arXiv:2209.05203](#)].
- [49] Y.Z. You, Z. Yang and X.L. Qi, *Machine Learning Spatial Geometry from Entanglement Features*, *Phys. Rev. B* **97** (2018) 045153 [[arXiv:1709.01223](#)].
- [50] H.Y. Hu, S.H. Li, L. Wang and Y.Z. You, *Machine Learning Holographic Mapping by Neural Network Renormalization Group*, *Phys. Rev. Res.* **2** (2020) 023369 [[arXiv:1903.00804](#)].
- [51] X. Han and S.A. Hartnoll, *Deep Quantum Geometry of Matrices*, *Phys. Rev. X* **10** (2020) 011069 [[arXiv:1906.08781](#)].
- [52] J. Lam and Y.Z. You, *Machine learning statistical gravity from multi-region entanglement entropy*, *Phys. Rev. Res.* **3** (2021) 043199 [[arXiv:2110.01115](#)].
- [53] M.M. Wolf, F. Verstraete, M.B. Hastings and J.I. Cirac, *Area Laws in Quantum Systems: Mutual Information and Correlations*, *Phys. Rev. Lett.* **100** (2008) 070502 [[arXiv:0704.3906](#)].
- [54] B.M. Terhal, M. Horodecki, D.W. Leung and D.P. DiVincenzo, *The entanglement of purification*, *J. Math. Phys.* **43** (2002) 4286 [[quant-ph/0202044](#)].

- [55] J. Couch, W. Fischler and P.H. Nguyen, *Noether charge, black hole volume, and complexity*, *JHEP* **03** (2017) 119 [[arXiv:1610.02038](#)].
- [56] A. Belin, R.C. Myers, S.M. Ruan, G.Sárosi and A.J. Speranza, *Does complexity equal anything?*, *Phys. Rev. Lett.* **128** (2022) 081602 [[arXiv:2111.02429](#)].
- [57] A.D. Polyinin, *Handbook of Integral Equations*, CRC Press. (1998)
- [58] W. Fischler, A. Kundu and S. Kundu, *Holographic mutual information at finite temperature*, *Phys. Rev. D* **87** (2013) 126012 [[arXiv:1212.4764](#)].
- [59] B. Swingle, *Mutual information and the structure of entanglement in quantum field theory*, *October 2010* [[arXiv:1010.4038](#)].
- [60] R. Espíndola, A. Guijosa and J.F. Pedraza, *Entanglement wedge reconstruction and entanglement of purification*, *Eur. Phys. J. C* **78** (2018) 646 [[arXiv:1804.05855](#)].
- [61] S. Bagchi and A.K. Pati, *Monogamy, polygamy, and other properties of entanglement of purification*, *Phys. Rev. A* **91** (2015) 042323 [[arXiv:1502.01272](#)].
- [62] P. Caputa, M. Miyaji, T. Takayanagi, K. Umemoto, *Holographic entanglement of purification from conformal field theories*, *Phys. Rev. Lett.* **122** (2019) 111601 [[arXiv:1812.05268](#)].
- [63] T. Takayanagi and K. Umemoto, *Entanglement of purification through holographic duality*, *Nature Phys.* **14** (2018) 573 [[arXiv:1708.09393](#)].
- [64] K. Tamaoka, *Entanglement Wedge Cross Section from the Dual Density Matrix*, *Phys. Rev. Lett.* **122** (2019) 141601 [[arXiv:1809.09109](#)].
- [65] R.Q. Yang, C.Y. Zhang and W.M. Li, *Holographic entanglement of purification for thermofield double states and thermal quench*, *JHEP* **01** (2019) 114 [[arXiv:1810.00420](#)].
- [66] J. Watrous, *Quantum Computational Complexity*, [[arXiv:0804.3401](#)].
- [67] A.R. Brown, D.A. Roberts, L. Susskind, B. Swingle and Y. Zhao, *Holographic Complexity Equals Bulk Action?*, *Phys. Rev. Lett.* **116** (2016) 191301 [[arXiv:1509.07876](#)].
- [68] D. Carmi, R.C. Myers and P. Rath, *Comments on Holographic Complexity*, *JHEP* **03** (2017) 118 [[arXiv:1612.00433](#)].
- [69] D. Carmi, S. Chapman, H. Marrochio, R.C. Myers and S. Sugishita, *On the Time Dependence of Holographic Complexity*, *JHEP* **11** (2017) 188 [[arXiv:1709.10184](#)].
- [70] Y.S. An, R.G. Cai and Y. Peng, *Time Dependence of Holographic Complexity in Gauss-Bonnet Gravity*, *Phys. Rev. D* **98** (2018) 106013 [[arXiv:1805.07775](#)].
- [71] Wolfram Language and System Documentation Center. *Numerical Solution of Differential-Algebraic Equations*.
- [72] F. Omid, *Generalized Volume-Complexity For Two-Sided Holographic Violating Black Branes*, *JHEP* **01** (2023) 105 [[arXiv:2207.05287](#)].
- [73] A.R. Brown, D.A. Roberts, L. Susskind, B. Swingle and Y. Zhao, *Complexity, action, and black holes*, *Phys. Rev. D* **93** (2016) 086006 [[arXiv:1512.04993](#)].
- [74] P. Burda, R. Gregory and A. Jain, *Holographic reconstruction of bubble spacetimes*, *Phys. Rev. D* **99** (2019) 026003 [[arXiv:1804.05202](#)].
- [75] S. Hernández-Cuenca and G.T. Horowitz, *Bulk reconstruction of metrics with a compact space asymptotically*, *JHEP* **08** (2020) 108 [[arXiv:2003.08409](#)].

- [76] Simons foundation: *It from Qubit: Simons collaboration on quantum Fields, gravity and information*.
- [77] N. Bao, C. Cao, S. Fischetti and C. Keeler, *Towards Bulk Metric Reconstruction from Extremal Area Variations*, *Class. Quant. Grav.* **36** (2019) 185002 [[arXiv:1904.04834](#)].
- [78] C. Cao, X.L. Qi, B. Swingle and E. Tang, *Building Bulk Geometry from the Tensor Radon Transform*, *JHEP* **12** (2020) 033 [[arXiv:2007.00004](#)].
- [79] V.E. Hubeny, H. Maxfield, M. Rangamani and E. Tonni, *Holographic entanglement plateaux*, *JHEP* **08** (2013) 092 [[arXiv:1306.4004](#)].
- [80] V. Balasubramanian, B.D. Chowdhury, B. Czech and J. de Boer, *Entwinement and the emergence of spacetime*, *JHEP* **01** (2015) 048 [[arXiv:1406.5859](#)].
- [81] B. Freivogel, R. Jefferson, L. Kabir, B. Mosk and I.-S. Yang, *Casting shadows on holographic reconstruction*, *Phys. Rev. D* **91** (2015) 086013 [[arXiv:1412.5175](#)].
- [82] N. Jokela, A. Pönni, T. Rindlisbacher, K. Rummukainen and A. Salami, *Disentangling the gravity dual of Yang-Mills theory*, [[arXiv:2304.08949](#)].